On the Near-Inertial Resonance of the Atlantic Meridional Overturning Circulation

FLORIAN SÉVELLEC

Ocean and Earth Science, National Oceanography Centre Southampton, University of Southampton, Southampton, United Kingdom

JOËL J.-M. HIRSCHI AND ADAM T. BLAKER

National Oceanography Centre, Southampton, Southampton, United Kingdom

(Manuscript received 26 April 2013, in final form 5 August 2013)

ABSTRACT

The Atlantic meridional overturning circulation (AMOC) is a crucial component of the global climate system. It is responsible for around a quarter of the global northward heat transport and contributes to the mild European climate. Observations and numerical models suggest a wide range of AMOC variability. Recent results from an ocean general circulation model (OGCM) in a high-resolution configuration ($^1/_4°$) suggest the existence of superinertial variability of the AMOC. In this study, the validity of this result in a theoretical framework is tested. At a low Rossby number and in the presence of Rayleigh friction, it is demonstrated that, unlike a typical forced damped oscillator (which shows subinertial resonance), the AMOC undergoes both super- and subinertial resonances (except at low latitudes and for high friction). A dimensionless number Sr, measuring the ratio of ageo- to geostrophic forcing (i.e., the zonal versus meridional pressure gradients), indicates which of these resonances dominates. If $\mathrm{Sr} \ll 1$, the AMOC variability is mainly driven by geostrophic forcing and shows subinertial resonance. Alternatively and consistent with the recently published $^1/_4°$ OGCM experiments, if $\mathrm{Sr} \gg 1$, the AMOC variability is mainly driven by the ageostrophic forcing and shows superinertial resonance. In both regimes, a forcing of ± 1 K induces an AMOC variability of ± 10 Sv ($1\,\mathrm{Sv} \equiv 10^6\,\mathrm{m^3\,s^{-1}}$) through these near-inertial resonance phenomena. It is also shown that, as expected from numerical simulations, the spatial structure of the near-inertial AMOC variability corresponds to equatorward-propagating waves equivalent to baroclinic Poincaré waves. The long-time average of this resonance phenomenon, raising and depressing the pycnocline, could contribute to the mixing of the ocean stratification.

1. Introduction

The Atlantic meridional overturning circulation (AMOC) is a baroclinic circulation that, on zonal average, can be schematically described as a northward surface flow above a deep equatorward recirculation (Sévellec and Fedorov 2011). Because of the existence of stratification (mainly controlled by temperature; i.e., warm water on top of cold water), this baroclinic circulation transports heat northward. As they are transported northward, surface waters exchange heat with the atmosphere, warming the northern region of the North Atlantic (Gagosian 2003). This process contributes to the climate of this region and partially explains the mild climate of Europe [a shutdown of the AMOC could cool down Europe by 1–3 K; Stouffer et al. (2006)].

AMOC variability spans a wide range of time scales. For example, the reorganization of the AMOC has been identified as a source of millennial-scale variability (Broecker et al. 1990; McManus et al. 2004) through the Dansgaard–Oeschger events (Bond et al. 1997). Significant work has also been done on the Atlantic multidecadal oscillation and its link to the AMOC (Kushnir 1994; Delworth and Mann 2000; Frankcombe et al. 2008). On shorter time scales, recent observations of the AMOC have shown substantial sub- and interannual variability at 26.5°N (Cunningham et al. 2007). While the seasonally averaged AMOC mean and standard deviation are 17.4 ± 4.9 Sv ($1\,\mathrm{Sv} \equiv 10^6\,\mathrm{m^3\,s^{-1}}$) between April 2004 and April 2011 (McCarthy et al. 2012), the intra-annual variability has a peak-to-peak range of

Corresponding author address: Florian Sévellec, Ocean and Earth Science, University of Southampton, Waterfront Campus, European Way, Southampton, SO14 3ZH, United Kingdom.
E-mail: florian.sevellec@noc.soton.ac.uk

DOI: 10.1175/JPO-D-13-092.1

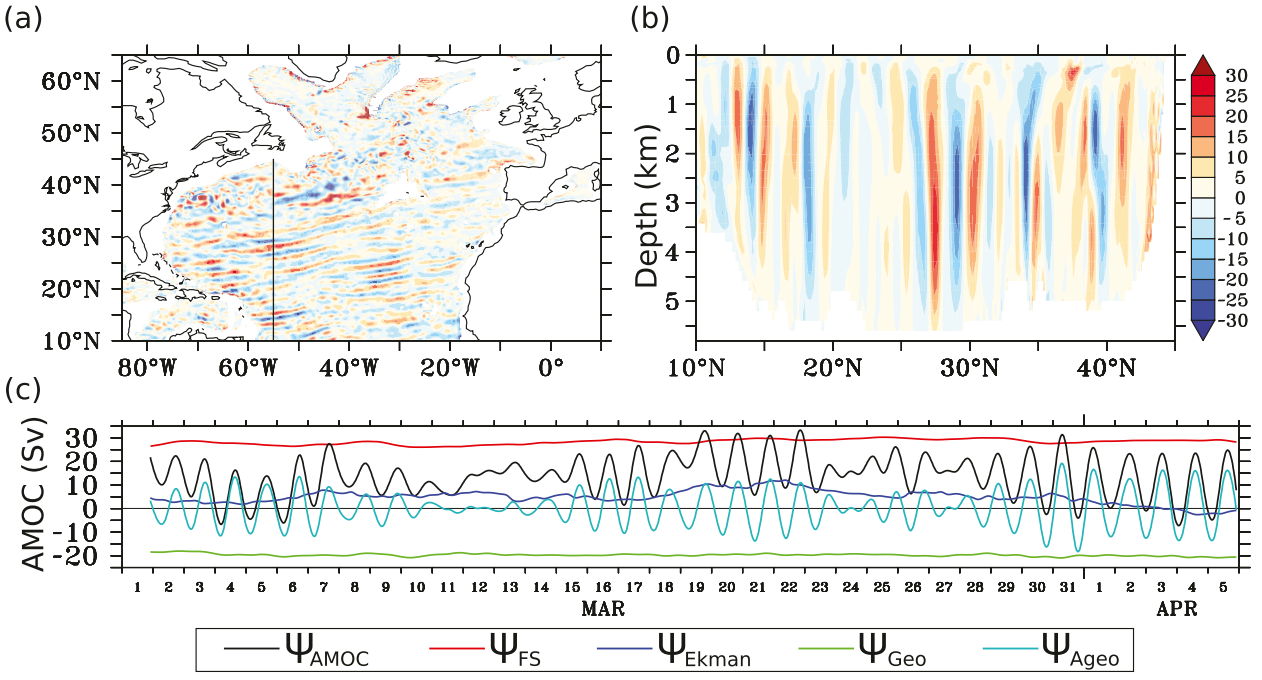

FIG. 1. Temporal and spatial characteristics of near-inertial variability in a 1/4° OGCM [Nucleus for European Modelling of the Ocean (NEMO) ORCA025; see Blaker et al. (2012), for further details]. Vertical velocities in the North Atlantic (m day^{-1}) are shown (a) at 2-km depth and (b) as a vertical section along 55°W, indicated by the black line in (a). (c) The strength of the AMOC and its components at 26.5°N are shown. The total AMOC Ψ_{AMOC} is split in to four terms: the Florida Strait component Ψ_{FS}, the Ekman component Ψ_{Ekman}, the geostrophic component Ψ_{Geo}, and the ageostrophic component Ψ_{Ageo}, the latter controlling the near-inertial variability. Time series show 4-hourly mean model output spline interpolated onto a 30-min grid.

30 Sv. From an oceanic perspective, this variability can be classified in two categories: the endo- and exogenous paradigms. In the endogenous paradigm, the source of the variability is internal ocean processes (e.g., Dijkstra and Ghil 2005). In the exogenous, the variability comes from an oceanic response to external perturbation, variability, or noise (e.g., Frankignoul and Hasselmann 1977). Although useful, this view is still an academic separation and the truth probably lies in the middle. For example, an internal mode of variability could be enhanced or partially sustained by an external forcing (Sévellec et al. 2009). Recently, Blaker et al. (2012) showed the existence of superinertial variability of the AMOC in a high-resolution (1/4°) OGCM. This variability is associated with equatorward-propagating waves exceeding 30 Sv of peak-to-peak amplitude (Fig. 1). This wave solution corresponds to positive and negative disturbances propagating along the pycnocline. Their work also suggests that this near-inertial variability is a response to surface momentum forcing, placing this study in an exogenous paradigm. The authors also suggest that this AMOC variability is nearly invisible to AMOC-observing systems such as Rapid Climate Change–Meridional Overturning Circulation (RAPID-MOC) at 26.5°N (Hirschi et al. 2003; Rayner et al. 2011).

Given this important limitation, we choose to apply a theoretical framework to confirm the existence of this variability. Starting from the typical set of primitive equations, at a low Rossby number and with Rayleigh friction for viscosity, we will demonstrate that the AMOC shows a superinertial resonance. Here, we consider density as the main forcing of the velocities. We assume that near-inertial variability exists in the density field and look at the AMOC response to these disturbances. With this assumption, we make the problem simpler as we no longer have to solve the full nonlinear problem arising through the advection–diffusion equation of density. Our approach has to be regarded as a first step toward a more general understanding. In this configuration, we will demonstrate that the zonally averaged momentum equations, and thus the AMOC, show optimal responses at sub- and superinertial frequencies (at least at high latitudes or for low friction). The former is induced by the geostrophic forcing (the east–west density difference), whereas, as suggested by Blaker et al. (2012), the latter derives from the ageostrophic driver of the AMOC (the zonally averaged meridional density gradient; Fig. 1). To

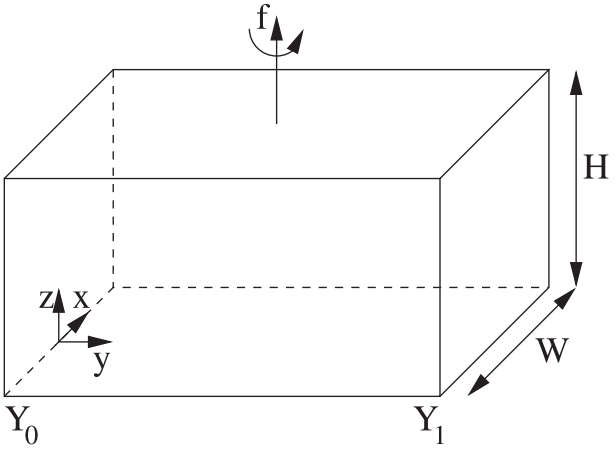

FIG. 2. Configuration of the idealized basin where x, y, and z are the zonal, meridional, and vertical coordinates. The zonal width is W, the depth is H, the local Coriolis parameter is f, and the latitude of the south- and northward boundaries are y_0 and y_1, respectively (see Table 1 for parameter values).

measure the dominant resonances we introduce a dimensionless number Sr, which is the ratio of ageo- to geostrophic forcing, and which indicates the dominating resonance. We will also show that this near-inertial variability is associated with an equatorward propagation of baroclinic Poincaré waves for regions away from the pycnocline slope.

The structure of the paper is as follows. In section 2, we describe the set of equations and the theoretical model configuration. In section 3, we show the existence of resonance in the AMOC. We also show that this resonance is sub- or superinertial when driven by the geo- or ageostrophic forcing of the AMOC, respectively. The propagating features associated with this variability are described in section 4, where we introduce an idealized setting for our equations (a 1.5-layer shallow water model). Discussion, conclusions, and directions for future work are given in section 5.

2. The set of equations and model configuration

The theoretical model consists of a flat bottom rectangular basin representing the North Atlantic (from $y_0 = 10°$N to $y_1 = 70°$N). The depth of the ocean $H = 4500$ m and its zonal extent $W = 4000$ km. However, as it will be demonstrated, the locality of the result and our approach means no assumptions regarding the basin shape or the topography are required. The rotation rate varies to represent the curvature of the earth (Fig. 2). In general, we will consider this ocean with stratification due to the density field. However, because our goal is not to solve the steady state, or the asymptotic solution, we do not need to explicitly consider the stratification

TABLE 1. Parameter values of the model.

y_0	10°N	Southern basin boundary
y_1	70°N	Northern basin boundary
H	4500 m	Total ocean depth
W	4000 km	Zonal basin extent
g	$9.8\,\mathrm{s}^{-2}$	Acceleration due to gravity
ρ_0	$1027\,\mathrm{kg\,m}^{-3}$	Reference density
ϵ	$1, 2, 5, 10 \times 10^{-5}\,\mathrm{s}^{-1}$	Linear friction coefficient
$\overline{h}$	1000 m	Zonally averaged pycnocline depth
ΔT	24 K	Temperature difference
ΔS	1.2 psu	Salinity difference
α	$2 \times 10^{-4}\,\mathrm{K}^{-1}$	Thermal expansion coefficient
β	$7 \times 10^{-4}\,\mathrm{psu}^{-1}$	Haline contraction coefficient

(except in section 4, where reduced gravity is defined). Description of the asymptotic solution can be found in Sijp et al. (2012). We also refer the reader to Kawase (1987) and Johnson and Marshall (2002), who described how such a steady state is achieved.

To represent this model and given the large scale of the AMOC, we neglect the nonlinear terms in the momentum equation (Ro $\ll 1$, where Ro is the Rossby number, measuring the ratio of inertial to Coriolis terms in the momentum equations). The viscosity will be specified by Rayleigh friction in the horizontal momentum equations. Furthermore, we use the hydrostatic approximation, a linear equation of state, and prescribe nondivergence. This set of equations, described by Salmon (1998) as the noninertial ocean dynamics, can be mathematically described in Cartesian coordinates by

$$\partial_t u - fv = -\frac{1}{\rho_0}\partial_x P - \epsilon u, \tag{1a}$$

$$\partial_t v + fu = -\frac{1}{\rho_0}\partial_y P - \epsilon v, \tag{1b}$$

$$\partial_z P = -\rho g, \tag{1c}$$

$$\rho = \rho_0[1 - \alpha(T - T_0) + \beta(S - S_0)], \quad \text{and} \tag{1d}$$

$$\partial_x u + \partial_y v + \partial_z w = 0, \tag{1e}$$

where x, y, and z are the three spatial coordinates; ρ_0, T_0, and S_0 are reference density, temperature, and salinity; α is the coefficient of thermal expansion; β is the coefficient of haline contraction; f is the Coriolis parameter; ϵ is the linear friction coefficient; T is the temperature; S is the salinity; P is the pressure; ρ is the density; and u, v, and w are the zonal, meridional, and vertical velocities (see Table 1 for parameter values).

In this set of equations, a friction term should be retained in the vertical momentum balance: $\partial_z P = -\rho g - \rho_0 \lambda w$, where λ is the vertical friction coefficient (Salmon 1998).

This term is fundamental to allow boundary conditions such as no heat flux ($\partial_n \rho = 0$, where n is the coordinate of the direction normal to the local boundary) together with rigid boundary ($u_n = 0$, where u_n is the velocity normal to the local boundary). This means that, at the boundary, the vertical velocity would be important to balance the pressure gradient: $\partial_n w|_{n=0} = \partial_z \partial_n P|_{n=0}/(\lambda \rho_0)$. In the absence of this vertical friction, the no heat flux and rigid boundary condition necessarily imposes the pressure to be adjusted all along the boundary ($\partial_n P|_{n=0} = 0$). In a closed basin, this filters out AMOC dynamics [for a more extensive discussion and numerical integrations, we refer the reader to the study of Huck et al. (1999)]. However, to the first order, and because we will not prescribe heat transfer at the horizontal boundaries, one could neglect this friction term and apply the hydrostatic approximation: $\partial_z P = -\rho g$.

3. Resonance of the AMOC

a. Zonal averaging

Applying the hydrostatic approximation to the vertical derivative of the two horizontal momentum equations leads to

$$[f^2 + (\partial_t + \epsilon)^2]\partial_z u = f\frac{g}{\rho_0}\partial_y \rho + \frac{g}{\rho_0}(\partial_t + \epsilon)\partial_x \rho \quad \text{and} \quad (2a)$$

$$[f^2 + (\partial_t + \epsilon)^2]\partial_z v = -f\frac{g}{\rho_0}\partial_x \rho + \frac{g}{\rho_0}(\partial_t + \epsilon)\partial_y \rho. \quad (2b)$$

We first define the zonal average of any variable X such that $\overline{X} = 1/W \int_{x_W}^{x_E} X\, dx$, where dx is the zonal unit coordinate, $W = x_E - x_W$ is the zonal basin extent, and x_E and x_W are the east and west zonal boundary limit of the basin, respectively. Applying this zonal averaging, (2b) becomes

$$[\partial_t^2 + 2\epsilon\partial_t + (f^2 + \epsilon^2)]\partial_z \overline{v} = \frac{fg}{W\rho_0}(\rho|_{x_W} - \rho|_{x_E}) + \frac{g}{\rho_0}(\epsilon + \partial_t)\partial_y \overline{\rho}. \quad (3)$$

This equation corresponds to a second-order nonautonomous differential equation.

Given the linearity of this equation, we split the solution in two terms: a geostrophic (keeping only the first term on the right-hand side, which drives the geostrophic part of the AMOC) and ageostrophic (keeping only the second term on the right-hand side, which drives the ageostrophic part of the AMOC) part. This leads to two equations:

$$[\partial_t^2 + 2\epsilon\partial_t + (f^2 + \epsilon^2)]\partial_z \overline{v}_g = \frac{fg}{W\rho_0}(\rho|_{x_W} - \rho|_{x_E}) \quad \text{and} \quad (4a)$$

$$[\partial_t^2 + 2\epsilon\partial_t + (f^2 + \epsilon^2)]\partial_z \overline{v}_a = \frac{g}{\rho_0}(\epsilon + \partial_t)\partial_y \overline{\rho}, \quad (4b)$$

where the indices g and a on the meridional velocities indicate whether the geo- or ageostrophic part of the right-hand side of (3) has been kept, respectively (so that $\overline{v} = \overline{v}_g + \overline{v}_a$).

We use this last set of equations to study the AMOC response to disturbances in the density field. This approach simplifies the problem, preventing us from solving the full nonlinear problem arising through the advection–diffusion equation of density. However, it has to be regarded as a first step toward a more general understanding, which is partially developed in section 4.

To test the AMOC response to density field variation, we assume that the density field can be split into a time-mean and a time-varying component following a sinusoidal oscillation: $\overline{\rho} = \overline{\rho}_m + \overline{\rho}_v \cos(\Omega t)$, where $\overline{\rho}_m$ is the time-mean density, $\overline{\rho}_v$ is the intensity of the time variation of density, and Ω is the angular frequency of this density variation; and $\rho|_{x_W} - \rho|_{x_E} = (\tilde{\rho}) = \tilde{\rho}_m + \tilde{\rho}_v \cos(\Omega t)$, where $\tilde{\rho}$ is the east–west density difference, $\tilde{\rho}_m$ is the time-mean density difference, and $\tilde{\rho}_v$ is the intensity of time variation of the density difference. In general, the density field varies over a range of frequencies. Here, we restrict the density variation to a single frequency to determine how each individual frequency stimulates the AMOC.

Because of the linearity of (4a) and (4b), the general solutions can be split into three solutions ($\mathcal{S}_m^{g,a}, \mathcal{S}_i^{g,a}$, and $\mathcal{S}_v^{g,a}$), depending on the characteristics of the density field: $\tilde{\rho} = \tilde{\rho}_m$ or $\overline{\rho} = \overline{\rho}_m$, $\tilde{\rho} = 0$ or $\overline{\rho} = 0$, and $\tilde{\rho} = \tilde{\rho}_v \cos(\Omega t)$ or $\overline{\rho} = \overline{\rho}_v \cos(\Omega t)$ (where $\mathcal{S}_m^{g,a}$ is the shear due to time-mean density, $\mathcal{S}_i^{g,a}$ is shear due to initial condition, and $\mathcal{S}_v^{g,a}$ is the shear due to time variation of the density field using the geo- or ageostrophic forcing, respectively). The general solution of (3) is the superposition of all the components: $\mathcal{S} = \mathcal{S}^g + \mathcal{S}^a$ with $\mathcal{S}^{g,a} = \mathcal{S}_m^{g,a} + \mathcal{S}_i^{g,a} + \mathcal{S}_v^{g,a}$, where $\mathcal{S}^{g,a} = -W\partial_z \overline{v}_{g,a}$.

b. The geostrophic solution

Using (4a), the solution of the time-mean density field ($\rho|_{x_W} - \rho|_{x_E} = \tilde{\rho}_m$) can be obtained as an asymptotic ($t \to +\infty$) solution. It corresponds to

$$\mathcal{S}_m^g = -f\frac{g}{\rho_0}\tilde{\rho}_m. \quad (5)$$

This relates the shear to the meridional density gradient in a similar way to the thermal wind equation. Given that this equation is constant in time, this expression is a solution of (4a) at any time (not only asymptotically). This result is equivalent to the classical formulation

of the strength of the AMOC used by Hirschi and Marotzke (2007), in the context of RAPID-MOC.

The response to the initial conditions can be obtained by setting the forcing, the right-hand side of (4a), to zero:

$$[\partial_t^2 + 2\epsilon\partial_t + (f^2+\epsilon^2)]\mathcal{S}_i^g = 0. \tag{6}$$

Applying a solution of the form of an exponential: $\mathcal{S}_i = \mathcal{S}_i^0 \exp(\gamma t)$ (where $\mathcal{S}_i^0$ is the amplitude of the wave and γ is time evolution characteristic), we obtain

$$\gamma^2 + 2\epsilon\gamma + (f^2+\epsilon^2) = 0. \tag{7}$$

Here, γ admits two solutions: $\gamma_\pm = -\epsilon \pm if$. Thus, the general solution of the shear due to initial conditions is

$$\mathcal{S}_i^g = e^{-\epsilon t}[C_1\cos(ft) + C_2\sin(ft)], \tag{8}$$

where C_1 and C_2 are two constants set by the initial conditions. This corresponds to a damped oscillation of e-folding time scale $1/\epsilon$ and of period $2\pi/f$. This is the adjustment of the momentum equation to the steady state due to an initial disturbance. In the absence of time-dependent forcing ($\partial_t\tilde{\rho} = 0$), the general solution would be $\mathcal{S}_m^g + \mathcal{S}_i^g$, where the unknown of $\mathcal{S}_i^g$ is given by the initial conditions.

The response of the shear to time-varying density forcing follows the equation

$$[\partial_t^2 + 2\epsilon\partial_t + (f^2+\epsilon^2)]\mathcal{S}_v^g = -f\frac{g}{\rho_0}\tilde{\rho}_v\cos(\Omega t). \tag{9}$$

This equation has a solution of the form of

$$\mathcal{S}_v^g = \frac{f}{\sqrt{4\epsilon^2\Omega^2 + (\epsilon^2+f^2-\Omega^2)^2}}\frac{g}{\rho_0}\tilde{\rho}_v\cos(\Omega t). \tag{10}$$

The most general solution of (4a) being the addition of the three components: $\mathcal{S}^g = \mathcal{S}_m^g + \mathcal{S}_v^g + \mathcal{S}_i$. In the rest of the study, we focus primarily on the variable part (i.e., $\mathcal{S}_v^g$). We will describe how the vertical shear responds to the different forcing frequencies.

This solution shows that the amplitude of the response depends on the frequency of the forcing as expected from a forced damped oscillator (Fig. 3).

Now that we have an expression for the response of the shear, we estimate the forcing frequency leading to the maximum response. For that we apply $\partial_\Omega A_g = 0$, where A_g is the amplitude of the shear response driven by the geostrophic variability (i.e., $\tilde{\rho}_v$), that is, the constant part in (10). This leads to

$$\Omega_R^g = f\sqrt{1-\left(\frac{\epsilon}{f}\right)^2}, \quad \text{with} \quad f \geq \epsilon, \tag{11}$$

where Ω_R^g is the resonance angular frequency for the geostrophic forcing (the angular frequency for which the shear response is maximum; gray lines in Fig. 3). If $f < \epsilon$, there is no resonance (i.e., the resonance angular frequency goes to infinity). The independence of the resonance angular frequency owing to geostrophic forcing in (11) to both the width and total depth of the basin makes it particularly suited for comparison with the realistic GCM of Blaker et al. (2012). The amplitude of the resonance suggests that a variability of ± 1 K induces an AMOC response of ± 10 Sv ($= \pm A_g|_{\Omega_R^g}\overline{h}^2$, where $\overline{h} = 1000$ m is the typical zonally averaged pycnocline depth).

This last expression shows a resonance at subinertial frequency ($\Omega_R^g < f$), typical of a forced damped oscillator. This cannot explain the superinertial variability shown by Blaker et al. (2012). However, Blaker et al. (2012) show that in their model this superinertial behavior is an ageostrophic process (Fig. 1). As we will demonstrate in the next section, including the second term on the right-hand side of (3), leading to (4b), is crucial for the appearance of resonance at the superinertial frequency.

c. The ageostrophic solution

As described previously, the time-mean solution ($\overline{\rho} = \overline{\rho}_m$) of (4b) can be obtained as an asymptotic ($t \to +\infty$) solution. It corresponds to

$$\mathcal{S}_m^a = -\frac{\epsilon}{f^2+\epsilon^2}\frac{gW}{\rho_0}\partial_y\overline{\rho}_m. \tag{12}$$

This relates the shear to the meridional density gradient, in a similar way to a frictional balance. Given that this equation is constant in time, this expression is a solution of (4b) at any time (not only asymptotically).

Because the response to initial conditions could be obtained by setting the forcing, the right-hand side of (4b), to zero, the solution is $\mathcal{S}_i = \mathcal{S}_i^a = \mathcal{S}_i^g$. In the absence of time-dependent forcing ($\partial_t\rho = 0$) the general solution would be $\mathcal{S}_m^g + \mathcal{S}_m^a + \mathcal{S}_i$, where the unknown of $\mathcal{S}_i$ is given by the initial conditions.

The response of the shear to temporally variable density forcing follows the equation

$$[\partial_t^2 + 2\epsilon\partial_t + (f^2+\epsilon^2)]\mathcal{S}_v^a = -\frac{g}{W\rho_0}(\epsilon+\partial_t)\partial_y\overline{\rho}_v\cos(\Omega t) \quad \text{and} \tag{13}$$

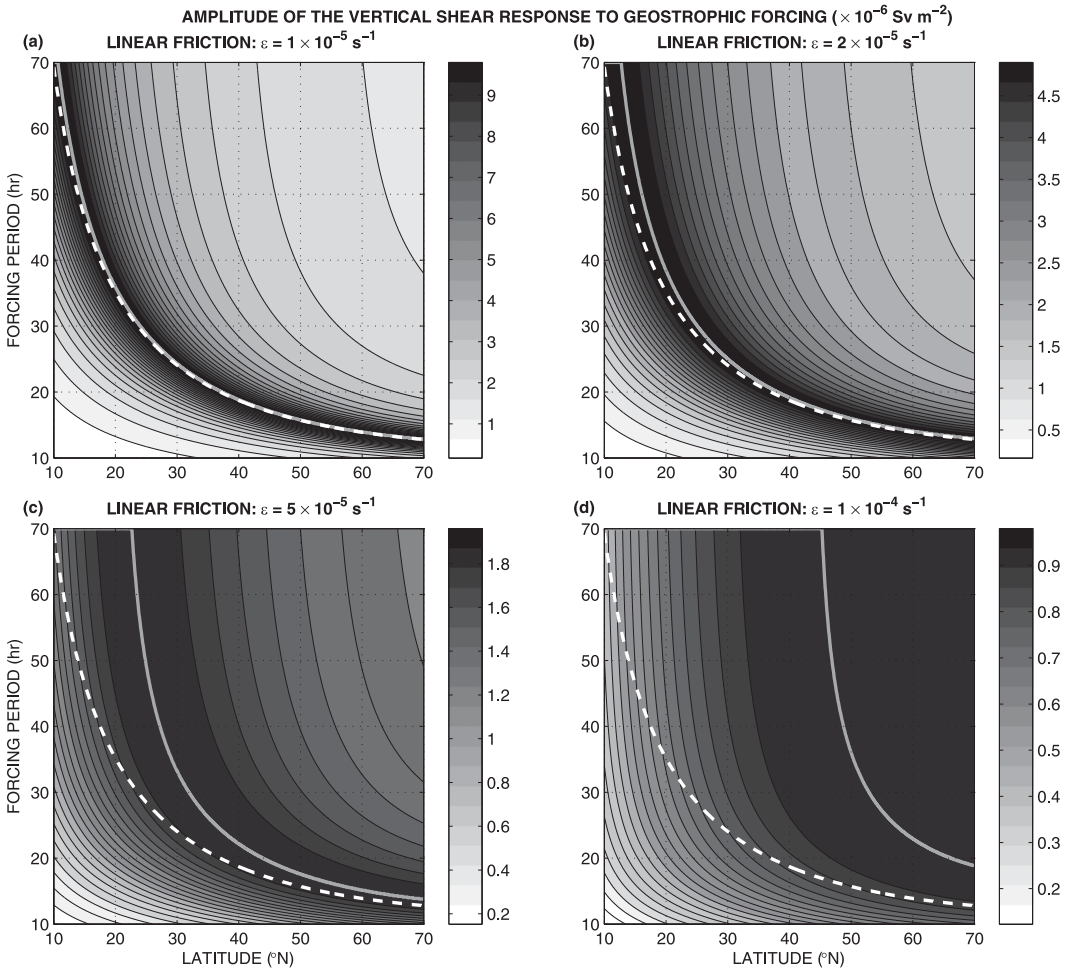

FIG. 3. Amplitude of the vertical shear response following (10) as a function of latitude and forcing period ($2\pi/\Omega$). (a)–(d) Four different values of the friction coefficient (ϵ = 1, 2, 5, and $10 \times 10^{-5}\,\mathrm{s}^{-1}$) are shown. Typical density variations are set to $\tilde{\rho}_v \sim 2 \times 10^{-2}\,\mathrm{kg\,m}^{-3}$ (i.e., 1 K). The gray lines represent the max response for each latitude and thus the resonance period Ω_R^g from (11) as a function of latitude. The dashed white line indicates the inertial period.

$$= -\frac{g}{W\rho_0}\sqrt{\epsilon^2+\Omega^2}\,\partial_y\overline{\rho}_v\cos(\Omega t+\phi), \qquad (14)$$

where ϕ is the phase delay between the density forcing and the shear response. This phase delay could be estimated exactly, but it is not needed for the purpose of this particular study. This equation has a solution of the form of

$$\mathcal{S}_v^a = \sqrt{\frac{\epsilon^2+\Omega^2}{4\epsilon^2\Omega^2+(\epsilon^2+f^2-\Omega^2)^2}}\,\frac{gW}{\rho_0}\,\partial_y\overline{\rho}_v\cos(\Omega t+\phi). \qquad (15)$$

The most general solution of (4b) is the addition of the three components: $\mathcal{S}^a = \mathcal{S}_m^a + \mathcal{S}_v^a + \mathcal{S}_i$. In the rest of the study, we focus primarily on the variable part (i.e., $\mathcal{S}_v^a$). We will describe how the vertical shear responds to the different forcing frequencies.

This solution shows that the amplitude of the response depends on the frequency of the forcing (Fig. 4).

Another interesting feature of the ageostrophic response is that unlike a typical forced damped oscillator, the amplitude of the forcing also depends on the forcing frequency, because of the ∂_t term in (4b). This obviously modifies the response. In other words, whereas from a typical forced damped oscillator we should expect a resonance at the subinertial frequency, we will demonstrate that our response is optimal at a superinertial frequency ($\Omega > f$).

Now that we have an expression for the response of the shear, we estimate the forcing frequency leading to the maximum response. For that we apply $\partial_\Omega A_a = 0$, where A_a is the amplitude of the shear response driven

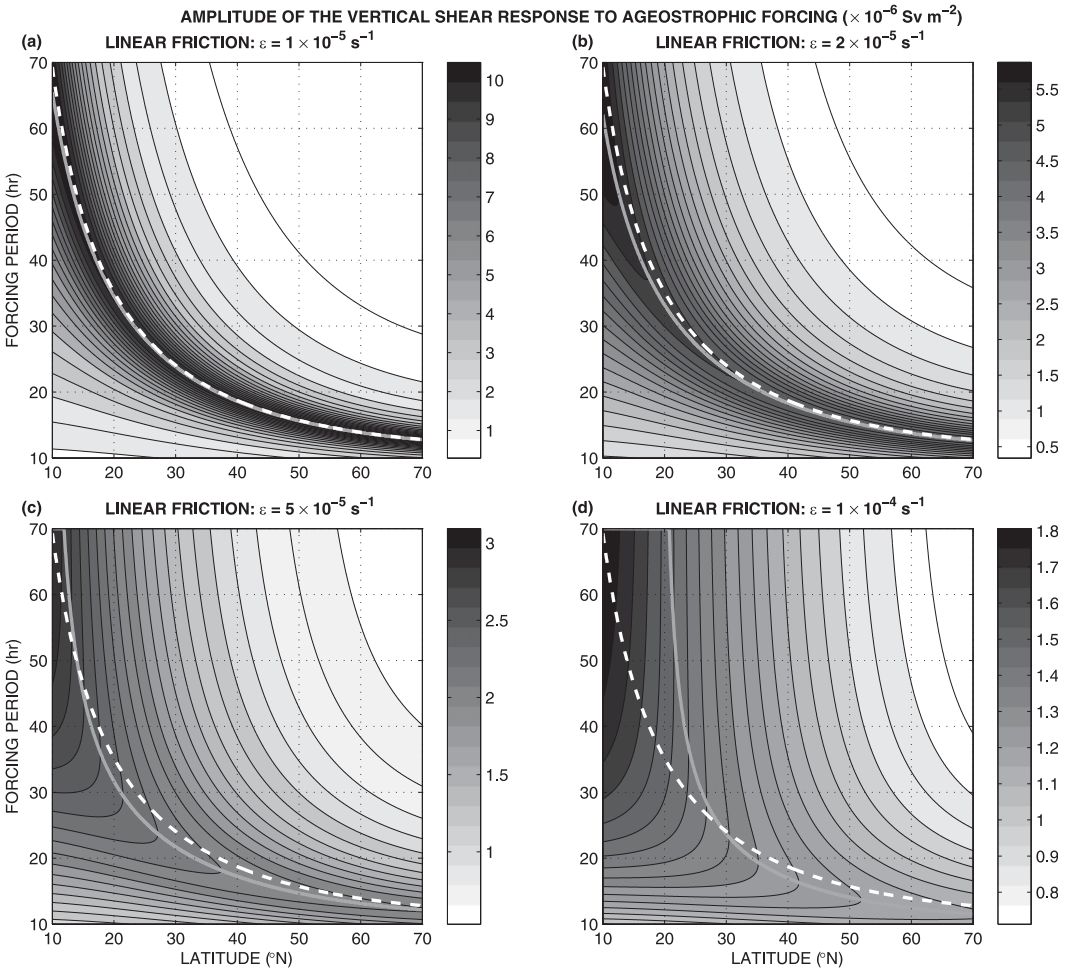

FIG. 4. As in Fig. 3, but for (15). Typical density variations are set to $W\partial_y\overline{\rho}_v \sim 2\times10^{-2}\,\mathrm{kg\,m^{-3}}$ (i.e., 1 K). The resonance period (Ω^a_R) is derived from (16).

by the ageostrophic variability (i.e., $\partial_y\overline{\rho}_v$), that is, the constant part in (15). This leads to

$$\Omega^a_R = f\sqrt{\sqrt{1+4\left(\frac{\epsilon}{f}\right)^2}-\left(\frac{\epsilon}{f}\right)^2}, \quad \text{with} \quad f \geq f_c, \tag{16}$$

where Ω^a_R is the resonance angular frequency (the angular frequency for which the shear response to the ageostrophic term is maximum; gray lines in Fig. 4), and f_c is a cutoff frequency such that $f_c^2 = (-2+\sqrt{5})\epsilon^2$. This cutoff frequency indicates that below a certain latitude (depending on friction), there is no resonance (i.e., the resonance angular frequency goes to infinity). The independence of the resonance angular frequency from ageostrophic forcing in (16) to both the width and total depth of the basin makes it particularly suited for comparison with the realistic GCM of Blaker et al. (2012). The amplitude of the resonance suggests that a variability of ±1 K induces an AMOC response of ±10 Sv ($=\pm A_a|_{\Omega^a_R}\overline{h}^2$, where $\overline{h}=1000$ m is the typical zonally averaged pycnocline depth).

We use this analytical expression to check if the resonance is super- or subinertial (i.e., if $\Omega^a_R > f$ or $\Omega^a_R < f$, respectively). To do so, we calculate the condition for an inertial resonance ($\Omega^i_R = f$, where Ω^i_R is the resonance angular frequency such that it is exactly inertial). We found the condition $f = \epsilon/\sqrt{2}$.

To summarize our results on the resonance of the vertical shear of the zonally averaged meridional velocity, we found three regimes depending on the latitude (and thus f) for a given friction. The resonance

- is superinertial for $f > \epsilon/\sqrt{2}$,
- is subinertial for $\epsilon\sqrt{-2+\sqrt{5}} \leq f < \epsilon/\sqrt{2}$, and
- does not exist for $f < \epsilon\sqrt{-2+\sqrt{5}}$.

At the edge between the first two regimes, for $f = \epsilon/\sqrt{2}$, the resonance is exactly inertial. In the case of low friction ($\epsilon < f$, such as we expect in the ocean, and

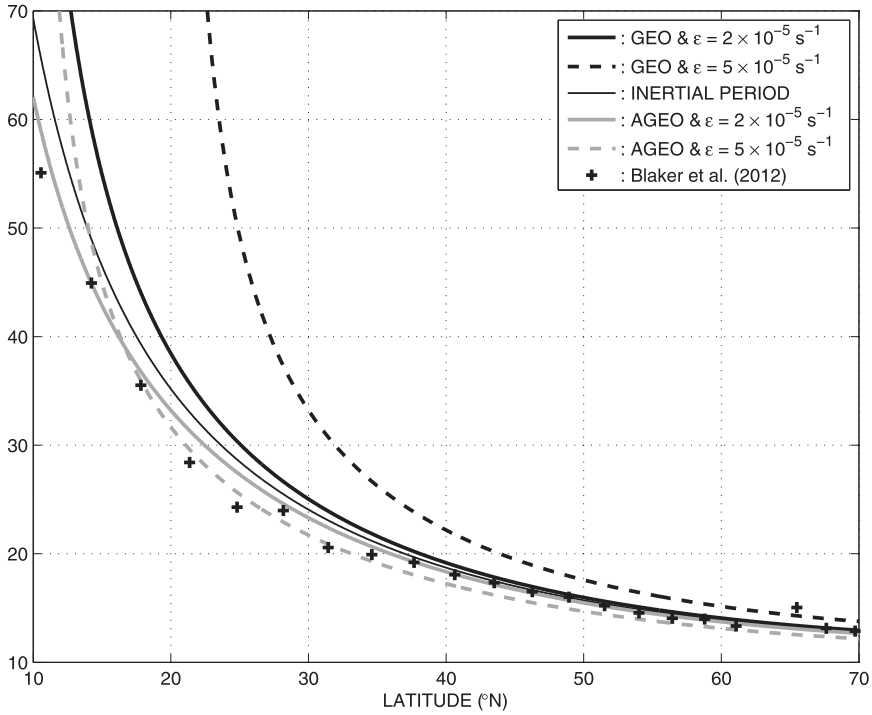

FIG. 5. Period of the max amplitude response of the vertical shear for the geo- (black lines) and ageostrophic (gray lines) terms following (11) and (16), respectively. Solid lines represent the result for $\epsilon = 2 \times 10^{-5}\,\mathrm{s}^{-1}$, the gray lines in Figs. 3b and 4b, respectively. Dashed lines represent the result for $\epsilon = 5 \times 10^{-5}\,\mathrm{s}^{-1}$, the gray lines in Figs. 3c and 4c, respectively. The thin black line indicates the inertial period. The crosses denote the AMOC variability period from the 1/4° OGCM experiments by Blaker et al. (2012).

thus in the 1/4° OGCM), the resonance is superinertial (Fig. 4b).

d. Geostrophic versus ageostrophic solutions

To determine if the resonance is super- or subinertial at least at high latitudes or for low friction, we have to compare the geo- and ageostrophic results [i.e., (10) versus (15)]. Assuming that the forcing frequency is on the order of the inertial frequency (i.e., $\Omega = f$), we can define a dimensionless number, the shear resonance Sr, measuring the ratio of the geo- to ageostrophic terms: $\mathrm{Sr} = W\partial_y\bar{\rho}_v/\tilde{\rho}_v$. Thus, at high latitudes or for low friction,

- if $\mathrm{Sr} \ll 1$, the geostrophic forcing dominates and the resonance is subinertial, and
- if $\mathrm{Sr} \gg 1$, the ageostrophic forcing dominates and the resonance is superinertial.

In their 1/4° OGCM experiment, Blaker et al. (2012) show that, at all latitudes, the superinertial resonance is associated with the ageostrophic term (Fig. 1), which is consistent with our result (Fig. 5).

Note that in the 1/4° OGCM the effective friction depends on the latitude because the grid is nonuniform (i.e., isotropic Mercator; Madec and Imbard 1996). For example, the extent of the zonal and meridional discretization is bigger at low latitudes. This corresponds to lower effective friction, that is, a smaller equivalent Rayleigh friction coefficient near the equator. This is also consistent with our findings. Between 20° and 30°N, the 1/4° OGCM behaves as the theoretical solution with $\epsilon = 5 \times 10^{-5}\,\mathrm{s}^{-1}$. Below 20°N, the OGCM behaves like $\epsilon = 2 \times 10^{-5}\,\mathrm{s}^{-1}$ (Fig. 5). At higher latitudes, the sensitivity of the solution to the friction intensity is weak and comparison becomes highly speculative. However, consistency between the numerical model and theoretical analysis remains.

On the limits of high Reynolds number ($\mathrm{Re} \gg 1$, i.e., friction is negligible), both geo- and ageostrophic forcings lead to inertial resonance. In other words, in higher-resolution models than the one used in Blaker et al. (2012), or in the real ocean, we could expect a resonance close to the inertial frequency.

4. Propagation of the AMOC variability

We next consider the spatial propagation of the AMOC variability for regions away from horizontal density gradients (i.e., outcropping regions).

We simplify the general set of equations given in (1). For this, we will not consider a general stratification but a 1.5-layer shallow water model (Pedlosky 1979). In this setting, the motion is purely baroclinic and the density gradient is limited to the jump between an upper layer and a motionless deep layer. This system can be described as

$$\partial_t u_u - f v_u = -g' \partial_x h - \epsilon u_u \quad \text{and} \tag{17a}$$

$$\partial_t v_u + f u_u = -g' \partial_y h - \epsilon v_u, \tag{17b}$$

where u_u and v_u are the vertically averaged zonal and meridional velocities in the upper layer, respectively; h is the thickness of the upper layer; and $g' = g\Delta\rho/\rho_0$ is the reduced gravity, where $\Delta\rho$ is the density difference between the upper and lower layers. Using the linear equation of state for seawater, this density difference can be decomposed in terms of temperature and salinity as $\Delta\rho/\rho_0 = -\alpha\Delta T + \beta\Delta S$, where ΔT and ΔS are the temperature and salinity differences, respectively (parameter values are given in Table 1).

Applying the same procedure as in the previous section to get the zonal average, we find for the meridional velocity component:

$$[\partial_t^2 + 2\epsilon\partial_t + (f^2+\epsilon^2)]\overline{v}_u = \frac{fg'}{W}(h|_{x_E} - h|_{x_W}) - g'(\partial_t + \epsilon)\partial_y \overline{h}. \tag{18}$$

The form of this equation is similar to (3), and $\overline{v}_u$ will thus have the same solution as shown in the previous section. However, in this section, we will combine this equation with the nondivergence to show the existence of propagating features in the zonally averaged velocity (i.e., the AMOC).

Using (1e) in a zonally averaged form ($\partial_y\overline{v} + \partial_z\overline{w} = 0$, where we assume solid boundary at the east and west of the basin), we can write the nondivergence in the upper layer as

$$\partial_t \overline{h} = \overline{h}\partial_y \overline{v}_u, \tag{19}$$

where we assume $\overline{w}|_{z=0} = 0$ (i.e., rigid-lid approximation, filtering out the external gravity waves).

Combining (18) and (19), we obtain

$$[\partial_t^2 + 2\epsilon\partial_t + g'\overline{h}\partial_y^2 + g'\partial_y\overline{h}\partial_y + (f^2+\epsilon^2)]\overline{v}_u = \frac{fg'}{W}(h|_{x_E} - h|_{x_w}) - \epsilon g'\partial_y\overline{h}. \tag{20}$$

In this section, we assume that we are away from the outcropping of the pycnocline (so that $\partial_y\overline{h} = 0$ and $h|_{x_W} = h|_{x_E}$). A consequence of this assumption is that we do not consider the forcing—the right-hand side of (20). In the ocean, these two processes are strongly coupled, because the production of pycnocline slope variation (eddies) is likely to occur where there is high level of potential energy (i.e., a strong slope of the pycnocline). Unlike the previous section that shows the response of the shear to variation in the density, in this section we will simply study the free propagation of the induced variability. In this context, (20) becomes

$$[\partial_t^2 + 2\epsilon\partial_t + g'\overline{h}\partial_y^2 + (f^2+\epsilon^2)]\overline{v}_u = 0. \tag{21}$$

Applying a solution of the form of $\exp(\gamma t)\exp(iky)$, we find $\gamma_\pm = -\epsilon \pm i\sqrt{f^2 + c^2k^2}$, where $c = \pm\sqrt{g'\overline{h}}$. Two typical length scales appear: the Rossby deformation radius $R_d = \sqrt{g'\overline{h}}/f$ and the e-folding propagation radius $R_p = \sqrt{g'\overline{h}}/\epsilon$. We can also define the angular frequency of the wave as $\omega = \pm f\sqrt{1 + (kR_d)^2}$. From this wave equation, we can determine the phase and group velocities ($c_p = \omega/k$ and $c_g = \partial_k\omega$, respectively):

$$c_p = \pm c\sqrt{1 + \frac{1}{(kR_d)^2}} \quad \text{and} \tag{22a}$$

$$c_g = \pm\frac{c}{\sqrt{1 + \frac{1}{(kR_d)^2}}}, \tag{22b}$$

The independence of the Poincaré waves phase velocity in (22a) to both the width and total depth of the basin makes it particularly suited for comparison with the realistic GCM of Blaker et al. (2012).

These solutions have two limits. For short wavelengths ($R_d \gg 1/k$), the propagation is nondispersive and follows internal gravity waves ($c_g = c_p = c$). For long wavelengths ($R_d \ll 1/k$), the wave follows the inertial waves and they are dispersive with $c_g = 0$ and $c_p = \pm f/k$.

In the study of (Blaker et al. 2012), the waves are generated around 40°N in regions of intense eddy activity with a typical wavelength of 5°. The crests of this wave should thus propagate southward with a velocity, typical of internal gravity wave, of roughly 12.5 m s^{-1}. They should then slow down reaching roughly 4.8 m s^{-1} at 20°N. The slowdown is due to the decrease in the Coriolis parameter as the wave moves southward, and as a consequence the waves feel the gravity wave regime more intensely. These theoretical wave velocities (Fig. 6) are consistent with the propagation of the near-inertial wave described in the OGCM (Blaker et al. 2012) taking roughly 15 days for a crest to go from 40° to 10°N.

At the equator, the Poincaré waves are equivalent to nondispersive internal gravity waves. In this regime, they can cross the equator at a constant speed set solely

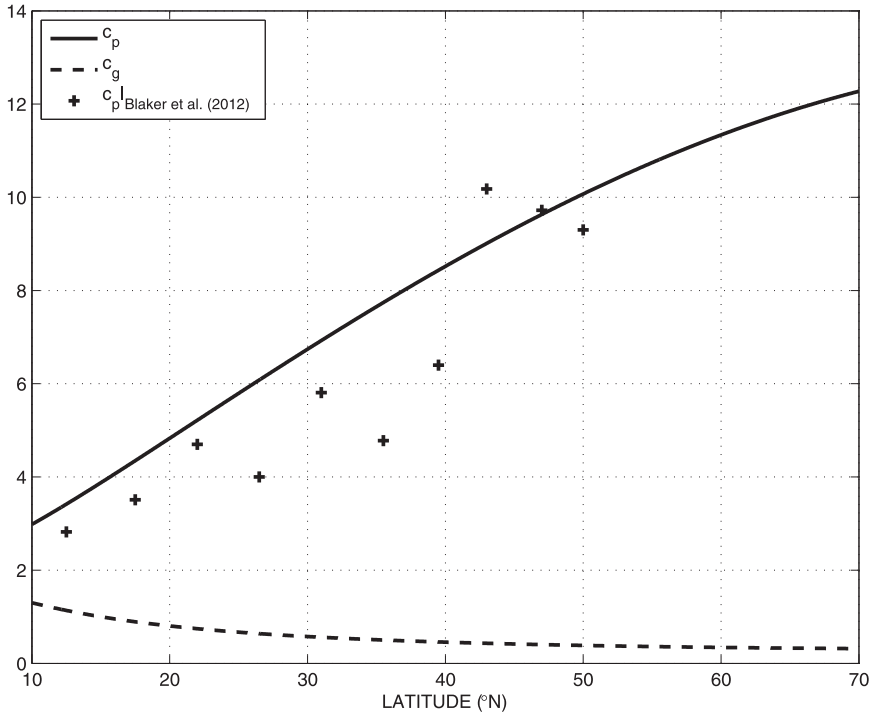

FIG. 6. Phase and group velocities [c_p (solid lines) and c_g (dashed lines), respectively] of the Poincaré waves for a 5° wavelength as a function of latitude. These results follow the analytical expression of (22), where a negative value of these curves is also a possible solution. The crosses denote the phase velocities from the ¼° OGCM experiments by Blaker et al. (2012).

by the stratification intensity. This behavior is consistent with new experiments (not shown) using the same ¼° OGCM as Blaker et al. (2012).

5. Conclusions

Although the existence of near-inertial variability in high-resolution ocean and coupled ocean–atmosphere models was determined by Fox et al. (2000) and Komori et al. (2008), its influence on the AMOC was only recently demonstrated by Blaker et al. (2012), who showed that the associated AMOC fluctuations can locally exceed 40 Sv (Fig. 1; whereas the long-time average is about 22.5 Sv). The authors showed that this variability is characterized by its superinertial signature and is associated with equatorward-propagating waves. From their experiments it is deduced that this high-frequency variability is an oceanic response to wind forcing, placing this variability in an exogenous paradigm. It was suggested by the authors that this variability is almost invisible to contemporary AMOC-observing systems (e.g., RAPID-MOC; Hirschi et al. 2003; Rayner et al. 2011). This current impossibility of testing such behavior against observational data stresses the importance of a theoretical study to validate the possibility of a superinertial response of the AMOC to external disturbances.

In this study, we use the momentum equations for small Rossby number (Ro $\ll$ 1, neglecting nonlinear advective terms) where viscosity is parameterized by a Rayleigh friction term. The other assumptions are the hydrostatic approximation and nondivergence. With this set of equations, we find a second-order nonautonomous differential equation for the vertical shear of the zonally averaged meridional velocity ($\mathcal{S} = -W\partial_z\overline{v}$). The forcing part of the differential equation is controlled by the density field ($\partial_y\overline{\rho}$ and $\rho|_{x_W} - \rho|_{x_E}$). With this assumption, we study how near-inertial variability in the density field can force an AMOC response. Our approach cannot explain how these density disturbances appear in the ocean, though we note that Blaker et al. (2012) have shown that this near-inertial variability takes its source in the wind variability. As mentioned earlier, our study should be considered as a first step toward a more general understanding.

Assuming that each forcing term can be split into a time-mean and an oscillatory component (of angular frequency Ω), the general solution for the shear can be split into three parts: (i) one due to the initial conditions,

(ii) one due to the time-mean forcing, and (iii) one due to the oscillatory forcing. From this decomposition, we found an analytical solution for the variable part of the shear.

Using this analytical solution, we were able to find two optimal forcing frequencies (i.e., frequencies for which the shear shows the maximum response intensity). Which of these frequencies dominates is determined by the form of the forcing term of the AMOC, that is, geo- versus ageostrophic. If the forcing is mainly controlled by the geostrophic term, the ocean shows subinertial resonance, like typical frictional systems. However, if the forcing is dominated by the ageostrophic term, the resonance frequency reveals a striking result. The ocean shows a superinertial resonance (except at low latitudes and for high friction). This is a direct consequence of the shear being forced not only by the stratification but also by its time derivative. This last result is consistent with a high-resolution OGCM analysis (Blaker et al. 2012), where the AMOC shows superinertial resonance that the authors relate to the ageostrophic term. In both cases, the amplitude of the resonance suggests that a variability of ± 1 K induces an AMOC response of ± 10 Sv. This is almost 10 times as big as a direct geostrophic response (i.e., without retaining the accelerating terms in the horizontal momentum equations).

In the last part of the study, we used a 1.5-layer shallow water model to test the propagation of the variability. We demonstrate that, away from isopycnal outcropping (where the waves are generated in a high-resolution OGCM), anomalies propagate southward as baroclinic Poincaré waves. This means that these waves will cross the equator at a constant speed (set solely by the stratification intensity) as nondispersive internal gravity waves.

To synthesize, Poincaré waves, generated in the outcropping region of the North Atlantic and propagating southward, are able to stimulate an intense response of the AMOC through sub- or superinertial resonance (for geo- or ageostrophic forcing, respectively).

The existence of resonance, and therefore of high vertical velocities, raising and depressing the pycnocline could yield breaking waves and be a source of mixing. Also, the Poincaré waves, which travel on a basin scale, could transport mass and energy away from the source of disturbance (potentially redistributing the energy input by the wind). These are the subject of ongoing research. In a recent study, near-inertial gravity waves were parameterized in a climate model and were found to deepen the ocean mixed layer by up to 30% (Jochum et al. 2013).

Several other high-resolution ocean and coupled GCMs (e.g., Fox et al. 2000; Komori et al. 2008) have been shown to reproduce this near-inertial variability. However, none of these studies have examined the influence of the waves on the time-mean ocean circulation. We will extend the work presented in this paper and test our theory with other high-resolution and coupled GCMs in a future study.

Acknowledgments. Florian Sévellec was supported by the Ti Ammo project funded through the French CNRS/INSU/LEFE program. Joel Hirschi and Adam Blaker were supported by the RAPID-WATCH project VALOR (NE/G007772/1). FS thanks Alain Colin de Verdière for useful comments on an early version of the manuscript. We thank two anonymous reviewers for their comments and suggestions.

REFERENCES

Blaker, A. T., J. J.-M. Hirschi, B. Sinha, B. de Cuevas, S. Alderson, A. Coward, and G. Madec, 2012: Large near-inertial oscillations of the Atlantic meridional overturning circulation. *Ocean Modell.,* **42,** 50–56.

Bond, G., and Coauthors, 1997: A pervasive millennial-scale cycle in North Atlantic Holocene and glacial climates. *Science,* **278,** 1257–1266.

Broecker, W. S., G. Bond, M. Klas, G. Bonani, and W. Wolfli, 1990: A salt oscillator in the glacial Atlantic? 1. The concept. *Paleoceanography,* **5,** 469–477.

Cunningham, S., and Coauthors, 2007: Temporal variability of the Atlantic meridional overturning circulation at 26.5°N. *Science,* **317,** 935–937.

Delworth, T. L., and M. E. Mann, 2000: Observed and simulated multidecadal variability in the Northern Hemisphere. *Climate Dyn.,* **16,** 661–676.

Dijkstra, H. A., and M. Ghil, 2005: Low-frequency variability of the large-scale ocean circulation: A dynamical systems approach. *Rev. Geophys.,* **43,** RG3002, doi:10.1029/2002RG000122.

Fox, A., K. Haines, and B. A. de Cuevas, 2000: Modelling internal waves with a global ocean model. *International WOCE Newsletter,* No. 39, WOCE International Project Office, Southampton, United Kingdom, 833–849.

Frankcombe, L. M., H. A. Dijkstra, and A. von der Heydt, 2008: Subsurface signatures of the Atlantic multidecadal oscillation. *Geophys. Res. Lett.,* **35,** L19602, doi:10.1029/2008GL034989.

Frankignoul, C., and K. Hasselmann, 1977: Stochastic climate models. Part II: Application to sea surface temperature anomalies and thermocline variability. *Tellus,* **29,** 289–305.

Gagosian, R. B., 2003: Abrupt climate change, should we be worried? *Proc. World Economic Forum,* Davos, Switzerland, Woods Hole Oceanographic Institution, 1–15.

Hirschi, J., and J. Marotzke, 2007: Reconstructing the meridional overturning circulation from boundary densities and the zonal wind stress. *J. Phys. Oceanogr.,* **37,** 743–763.

——, J. Baehr, J. Marotzke, J. Stark, S. Cunningham, and J.-O. Beismann, 2003: A monitoring design for the Atlantic meridional overturning circulation. *Geophys. Res. Lett.,* **30,** 1413, doi:10.1029/2002GL016776.

Huck, T., A. J. Weaver, and A. Colin de Verdière, 1999: On the influence of the parameterization of lateral boundary layers on

the thermohaline circulation in coarse-resolution ocean models. *J. Mar. Res.,* **57,** 387–426.

Jochum, M., B. P. Briegleb, G. Danabasoglu, W. G. Large, N. J. Norton, S. R. Jayne, M. H. Alford, and F. O. Bryan, 2013: The impact of oceanic near-inertial waves on climate. *J. Climate,* **26,** 2833–2844.

Johnson, H. L., and D. P. Marshall, 2002: A theory for the surface Atlantic response to thermohaline variability. *J. Phys. Oceanogr.,* **32,** 1121–1132.

Kawase, M., 1987: Establishment of deep ocean circulation driven by deep-water production. *J. Phys. Oceanogr.,* **17,** 2294–2317.

Komori, N., W. Ohfuchi, B. Taguchi, H. Sasaki, and P. Klein, 2008: Deep ocean inertia-gravity waves simulated in a high-resolution global coupled atmosphere–ocean GCM. *Geophys. Res. Lett.,* **35,** L04610, doi:10.1029/2007GL032807.

Kushnir, Y., 1994: Interdecadal variations in North Atlantic sea surface temperature and associated atmospheric conditions. *J. Climate,* **7,** 141–157.

Madec, G., and M. Imbard, 1996: A global ocean mesh to overcome the North Pole singularity. *Climate Dyn.,* **12,** 381–388.

McCarthy, G., and Coauthors, 2012: Observed interannual variability of the Atlantic meridional overturning circulation at 26.5°N. *Geophys. Res. Lett.,* **39,** L19609, doi:10.1029/2012GL052933.

McManus, J. F., R. Francois, J.-M. Gherardi, L. D. Keigwin, and S. Brown-Leger, 2004: Collapse and rapid resumption of Atlantic meridional circulation linked to deglacial climate changes. *Nature,* **428,** 834–836.

Pedlosky, J., 1979: *Geophysical Fluid Dynamics.* Springer-Verlag, 728 pp.

Rayner, D., and Coauthors, 2011: Monitoring the Atlantic meridional overturning circulation. *Deep-Sea Res.,* **12,** 1744–1753.

Salmon, R., 1998: *Lectures on Geophysical Fluid Dynamics.* Oxford University Press, 400 pp.

Sévellec, F., and A. V. Fedorov, 2011: Stability of the Atlantic meridional overturning circulation in a zonally averaged ocean model: The effects of freshwater flux, wind stress, and diapycnal diffusion. *Deep-Sea Res.,* **58,** 1927–1943.

——, T. Huck, M. B. Jelloul, and J. Vialard, 2009: Nonnormal multidecadal response of the thermohaline circulation induced by optimal surface salinity perturbations. *J. Phys. Oceanogr.,* **39,** 852–872.

Sijp, W. P., J. M. Gregory, R. Tailleux, and P. Spence, 2012: The key role of the western boundary in linking the AMOC strength to the north–south pressure gradient. *J. Phys. Oceanogr.,* **42,** 628–643.

Stouffer, R. J., and Coauthors, 2006: Investigating the causes of the response of the thermohaline circulation to past and future climate changes. *J. Climate,* **19,** 1365–1387.